Chronic reduction in inhibition reduces receptive field size in mouse auditory cortex

Bryan A. Seybold[a,1], Amelia Stanco[b], Kathleen K. A. Cho[c], Gregory B. Potter[b,d], Carol Kim[b], Vikaas S. Sohal[c], John L. R. Rubenstein[b], and Christoph E. Schreiner[a]

[a]Coleman Memorial Laboratory, Department of Otolaryngology-Head and Neck Surgery, and [c]Department of Psychiatry, Center for Integrative Neuroscience, Sloan-Swartz Center for Theoretical Neurobiology, and [b]Nina Ireland Laboratory for Developmental Neurobiology, Department of Psychiatry, Center for Neurobiology and Psychiatry, Neuroscience Graduate Program, University of California, San Francisco, CA 94143; and [d]Department of Pediatrics, Oregon Health and Science University, Portland, OR 97239

Edited by Thomas D. Albright, The Salk Institute for Biological Studies, La Jolla, CA, and approved June 6, 2012 (received for review April 6, 2012)

Inhibitory interneurons regulate the responses of cortical circuits. In auditory cortical areas, inhibition from these neurons narrows spectral tuning and shapes response dynamics. Acute disruptions of inhibition expand spectral receptive fields. However, the effects of long-term perturbations of inhibitory circuitry on auditory cortical responses are unknown. We ablated ∼30% of dendrite-targeting cortical inhibitory interneurons after the critical period by studying mice with a conditional deletion of *Dlx1*. Following the loss of interneurons, baseline firing rates rose and tone-evoked responses became less sparse in auditory cortex. However, contrary to acute blockades of inhibition, the sizes of spectral receptive fields were reduced, demonstrating both higher thresholds and narrower bandwidths. Furthermore, long-latency responses at the edge of the receptive field were absent. On the basis of changes in response dynamics, the mechanism for the reduction in receptive field size appears to be a compensatory loss of corticocortically (CC) driven responses. Our findings suggest chronic conditions that feature changes in inhibitory circuitry are not likely to be well modeled by acute network manipulations, and compensation may be a critical component of chronic neuronal conditions.

Processing of auditory information in the auditory cortex underlies the conscious perception of sound and speech comprehension. Inhibitory interneurons, representing ∼20% of cortical neurons (1), regulate this processing by shaping the spectral tuning (2–13), temporal tuning (14–16), and response dynamics of local excitatory neurons (5–11). Inhibitory interneurons form multiple subtypes on the basis of morphology, physiology, and biochemistry (1, 17) that likely serve distinct roles in cortical processing.

Loss of inhibitory interneurons is observed in conditions that affect cortical processing in humans, and in animal models of human disorders, including aging (18, 19), autism (20), schizophrenia (21–23), traumatic brain injury (TBI) (24), hearing loss (25–28), and tinnitus (29). Often, a particular disease is associated with a specific deficit in a subset of interneurons. For example, rodent models of autism demonstrate a loss of parvalbumin positive (PV^+) interneurons (20), whereas aging and TBI models show a greater loss of somatostatin $(SST)^+$ interneurons than other interneuron populations (19, 24). The disruption of specific interneuron populations may underlie the particular cognitive defects associated with each condition. Therefore, it is necessary to understand the effects following chronic reductions of particular interneuron subtypes.

One mouse model of an adult-onset loss of dendrite-targeting interneurons (DTIs) is the *Dlx1* mutant (30). *Dlx1* encodes a homeobox transcription factor from the *Dlx* family that regulates the development, migration, and survival of cortical interneurons (30–32). In *Dlx1* mutants, the other *Dlx* family members compensate for the deficiency and thereby allow interneurons to migrate into cortex (30). At postnatal day 20 (p20) there is no observed loss of interneurons in *Dlx1* mutants; however by p30, ∼30% of SST^+, neuropeptide Y (NPY^+), and calretinin positive (CR^+) DTIs undergo apoptosis, whereas soma-targeting, PV^+ interneurons are unaffected (30). Following the loss of interneurons, the rate and size of spontaneous and miniature inhibitory postsynaptic potentials are reduced (30). Despite the normally broad expression of *Dlx1* in interneurons, there is no change in the intrinsic properties of the surviving interneurons after p30 (33). This partial loss of interneurons is similar to human adult-onset conditions that feature a selective loss of DTIs, such as aging and TBI, because the critical period for spectral tuning in auditory cortex ends before p20 in mice (34). *Dlx1* mutants are known to develop seizures, behavioral deficits, and abnormal visual cortical responses (35–37); however, changes in auditory processing are unknown.

Previous attempts to study the deficits in auditory cortical processing in a constitutive *Dlx1* knockout ($Dlx1^{-/-}$) were not successful because *Dlx1* also regulates the development of the middle ear ossicles (38, 39). The middle ear bones fuse in the absence of *Dlx1* and create a conductive hearing loss that raises auditory brainstem response (ABR) thresholds in $Dlx1^{-/-}$ mice by ∼30 dB, precluding a meaningful study of auditory cortical changes (38, 39). To circumvent this issue, we developed a conditional deletion of *Dlx1* restricted to forebrain GABAergic neurons using a floxed conditional allele of *Dlx1* and *DlxI12b-Cre* (*I12b-Cre*). *DlxI12b* is an enhancer element of *Dlx1* (40, 41). By placing Cre-recombinase under the control of this enhancer, which is not expressed in the primordia of the middle ear, recombination occurs in 95% of cortical interneurons (41). We will refer to these $Dlx1^{-/f}$;*I12b-Cre* animals as conditional knockout animals (cKO) and heterozygous littermates ($Dlx1^{+/f}$;*I12b-Cre*) as controls (CT).

Results

$Dlx1^{-/f}$;I12b-Cre Mice Lack a Subset of Dendrite-Targeting Interneurons. We validated the conditional deletion of *Dlx1* by confirming that the loss of dendrite-targeting interneurons (DTIs) in $Dlx1^{-/f}$;*I12b-Cre* (cKO) animals was consistent with the constitutive null mutants, $Dlx1^{-/-}$. As in $Dlx1^{-/-}$ mutants, ∼30% of dendrite-targeting, SST^+, NPY^+, and CR^+ interneurons were lost by p45 in cKO mice, whereas no change in the number of soma-targeting, PV^+ interneurons was observed (means ± STD labeled cells/mm^2: SST, CT 16.2 ± 1.0 and cKO, 10.4 ± 1.6, $P < 0.05$; NPY, CT 49.5 ± 2.5 and cKO 32.2 ± 3.4, $P < 0.05$; CR, CT 55.2 ± 1.5 and cKO 44.8 ± 3.0, $P < 0.05$; PV, CT 134.6 ± 5.6 and cKO 139.5 ± 5.6, $P >$

Author contributions: B.A.S., A.S., K.K.A.C., J.L.R.R., and C.E.S. designed research; B.A.S., A.S., and K.K.A.C. performed research; B.A.S., G.B.P., C.K., and V.S.S. contributed new reagents/analytic tools; B.A.S., A.S., and K.K.A.C. analyzed data; and B.A.S., A.S., K.K.A.C., G.B.P., J.L.R.R., and C.E.S. wrote the paper.

The authors declare no conflict of interest.

This article is a PNAS Direct Submission.

See Commentary on page 13473.

[1]To whom correspondence should be addressed. E-mail: bryan.seybold@ucsf.edu.

This article contains supporting information online at www.pnas.org/lookup/suppl/doi:10.1073/pnas.1205909109/-/DCSupplemental.

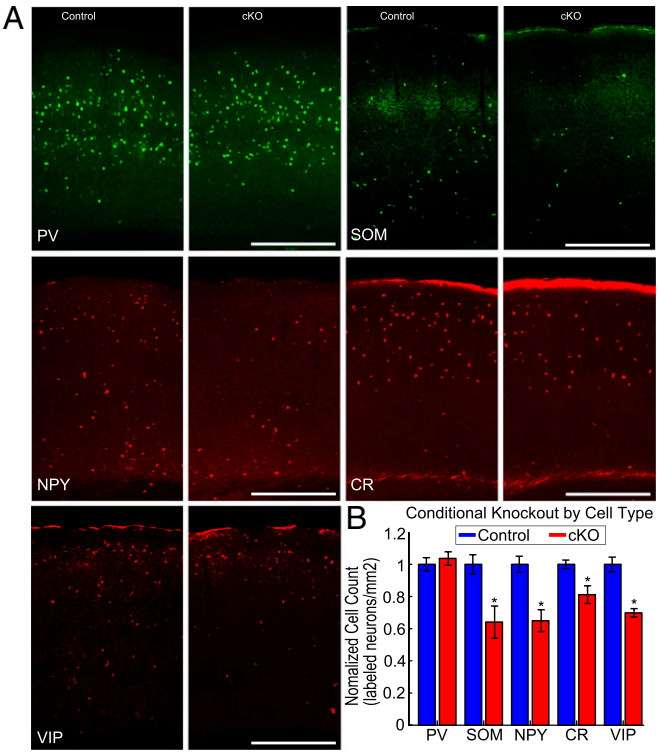

Fig. 1. Dendrite-targeting interneurons are reduced in cKO mutants. (*A*) Sections of auditory cortex from control and cKO mice labeled for various interneuron markers (from left to right, top to bottom: parvalbumin, somatostatin, neuropeptide Y, calretinin, vasoactive intestinal peptide). (*B*) Cell count in control and cKO mice: PV^+ ($P > 0.05$, $n = 3$ animals), SOM^+, NPY^+, CR^+, and VIP^+ interneurons ($P < 0.05$, $n = 3$ animals for each).

0.05; $n = 3$ animals each, Fig. 1 *A* and *B*). We extended the previous analysis to include vasoactive intestinal peptide positive (VIP^+) interneurons, which also displayed a 30% reduction in cKO mutants (mean ± STD labeled cells/mm^2: CT 42.2 ± 1.9 and cKO 29.5 ± 1.1, $P < 0.05$, $n = 3$ animals each). Similar to *Dlx1*$^{-/-}$ mice, cKO mutants displayed abnormal EEG activity (*SI Results* and Fig. S1*C*). The conditional knockout successfully avoided the elevated peripheral auditory thresholds of *Dlx1*$^{-/-}$ mice (38). The cKO mice, in contrast to *Dlx1*$^{-/-}$ mice, had normal ABR thresholds (medians: CT = 30 dB, cKO = 25 dB, $P = 0.17$, $n = 4$ and 3, Fig. S1 *A* and *B*). In sum, cKO mutants have the same selective loss of DTIs as the constitutive *Dlx1* mutant and develop a neurological condition independent of peripheral changes in the middle ear. Therefore, we used *Dlx1* cKO mutants to characterize changes in auditory cortex function that arise following the loss of DTIs.

Dlx1$^{-/f}$;I12b-Cre Cortical Units Have Restricted Receptive Fields. We determined the effect of the loss of DTIs on auditory processing by recording responses to pure tones and constructing frequency response areas (FRAs, firing rate as a function of tonal frequency and intensity, Fig. 2 *A*–*D*). We recorded from single-units in auditory cortical core areas, the primary auditory field (A1) and the anterior auditory field (AAF), across all cortical layers of cKO mutants ($n = 58$ units, eight animals) and controls ($n = 54$ units, eight animals) and quantified the size of the response area (area of FRA above 1/4 peak value), response threshold (lowest intensity in the response area), and spectral bandwidth (number of octaves responding at an intensity above threshold). In cKO cortical units, response area sizes were reduced (medians: CT = 177 dB*octaves, cKO = 144.5 dB*octaves, $P < 0.005$, Fig. 2*E* and Fig. S2*D*). This was a combined effect of higher thresholds (medians: CT = 20 dB, cKO = 25 dB, $P < 0.001$, Fig. 2 *C* and *F* and Fig. S2*E*) and narrower bandwidths (bandwidth at 20 dB above threshold: medians: CT = 1.1 octaves, cKO = 1.0 octave, uncorrected $P < 0.05$, Fig. 2 *D* and *G*, Fig. S2*F*; see *SI Results* for details of ANOVA). Contrary to the effects of acute, pharmacological blockades of inhibition, which broaden spectral tuning (6–12), the chronic loss of DTIs led to narrower spectral tuning, which is a reduction in receptive field size.

To test whether these changes emerge in cortex or are already present subcortically, we recorded single units across multiple divisions in the auditory thalamus (CT: 31 units from two animals; cKO, 65 units from three animals). In contrast to cortical FRAs, cKO and control thalamic FRA response areas were not significantly different (medians: CT = 109 dB*octaves, cKO = 142 dB*octaves, $P = 0.06$, Fig. 2*H* and Fig. S3; see *SI Results* for further characterization). Thus, the changes observed in cortex were not present in the thalamus—the preceding subcortical station—and likely arise in cortex.

Dlx1$^{-/f}$;I12b-Cre Cortical Units Respond with Altered Dynamics at the Edge of the Receptive Field. Cortical FRAs are driven by both cortico-cortical (CC) connections and thalamo-cortical (TC) connections. Whereas both TC and CC connections drive the center of the FRA [frequencies near the characteristic frequency (CF: frequency driving the response at threshold) and at high intensity] with short latencies, the edges of the FRA are primarily driven by CC connections with longer latencies (42–45). These CC inputs arrive later than TC inputs because they must travel through additional synapses and reflect both ongoing

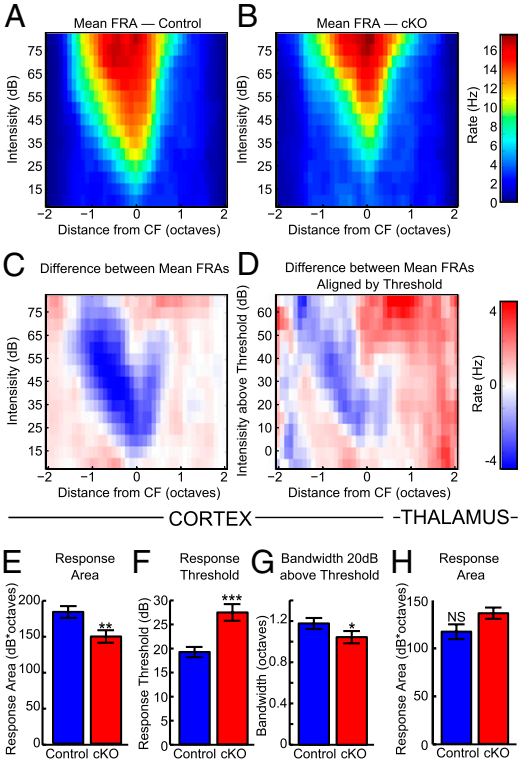

Fig. 2. Cortical spectral tuning area is reduced in cKO mutants. (*A* and *B*) the population mean FRAs aligned by CF for auditory cortical units. (*C*) Difference, cKO – control. (*D*) Difference with units aligned by threshold. (*E*–*G*) Size of responsive area of cortical units ($P < 0.01$, $P < 0.001$, and $P < 0.05$; $n = 54$ CT and 58 cKO). (*H*) Size of responsive area of thalamic units ($P > 0.05$; $n = 30$ CT and 61 cKO).

processes and horizontal cortical spread of activity (44, 45). Therefore, we measured the response dynamics at the center and edge of the FRA to explore how effectively CC connections drive activity in cKO mutants.

To quantify the response dynamics, we used peristimulus time histograms (PSTHs, Fig. 3*A–C*) for two different intensity regions near the characteristic frequency (CF ± 0.2 octaves when the description of CF was moved forward, this became redundant). To study the combined effect of TC and CC connections, the first PSTH was from stimuli in the center of the FRA at high intensities (60–80 dB, Fig. 3*E*). To focus on primarily CC-driven activity, the second PSTH was from the edge of the FRA at low intensities (threshold ± 10 dB, Fig. 3*F*). As with acute blockades of inhibition (6–12), baseline firing rates were higher in cKO units during the 50 ms preceding stimulus presentation and before driven responses began (medians: CT, 1.11 Hz and cKO, 2.38 Hz, $P < 0.005$, Fig. 3*D*). Beyond the change in baseline firing, there were no significant differences between cKO and control PSTHs at high intensities where both TC and CC inputs contribute [significance judged as at least five consecutive rank sum $P < 0.05$, in which case all consecutive, significant points are reported; values 0–9 ms (before the response onset of most units) pass this criterion, Fig. 3*E*]. In contrast, at low intensities where CC connections dominate, cKO responses begin earlier but are overtaken by control responses (cKO > CT, 0–16 ms; CT > cKO, 25–34 ms; at least five consecutive rank sum $P < 0.05$). In cKO mutants, responses driven by TC and CC connections appear to be normal in timing and rate, but baseline firing rates are higher and responses driven primarily by CC connections are abnormal in timing, magnitude, or both. We therefore quantified the response timing and response magnitude in greater detail.

Dlx1$^{-/f}$;I12b-Cre Cortical Units Lack Long-Latency Responses. To investigate the differences in temporal response dynamics for individual units, we quantified the response onset latency (time to half the peak height from baseline). The response latency of control units is longer at low intensities near threshold compared with high intensities (medians: CT-high = 15.5 ms, CT-low = 22 ms, Bonferroni corrected $P < 0.001$, Fig. 3*G*) in agreement with previous results where CC driven responses have longer latencies (44, 45). However, in cKO units, the response latency at low intensities occurs significantly earlier than in control units (medians: CT-low = 22 ms, cKO-low = 16 ms, Bonferroni corrected $P < 0.05$, Fig. 3*G*). Interestingly, Control latencies at high intensities were not significantly different from either high or low intensity latencies for cKO units (medians: CT-high = 15.5 ms, cKO-high = 12 ms, Bonferroni corrected $P > 0.05$; medians: CT-high = 15.5 ms, cKO-L = 16 ms, uncorrected $P = 0.31$, Fig. 3*G*). In other words, the response timing in cKO units at both high and low intensities was similar to central regions predominantly driven by TC connections in controls, and neither was similar to the primarily CC driven edge responses of controls. The response latencies for cKO units at low intensities were longer than at high intensities (medians: cKO-high = 12, cKO-low = 16 ms, Bonferroni corrected $P < 0.05$, Fig. 3*G*) presumably because the response latencies of subcortical stations are also stimulus intensity dependent (46). Therefore, receptive fields did not simply change shape, but the long-latency responses at low intensities normally driven by CC connections appeared to be absent in the cKO population.

To extend analysis of changes in response timing to the entire FRA, we calculated two short-time FRAs on the basis of 10-ms windows centered either on the response onset or response termination (termination: time at half the peak value after the peak response, Fig. 4 *A–C*). It has previously been shown (45) that the central, TC-driven FRA region becomes active first (Fig. 4*A*) and gives way to activity at the CC-driven edges of the FRA (Fig. 4*B*). Therefore, the FRA shapes from the response onset and termination should be negatively correlated. This correlation was observed for control units (median: −0.05, signed rank $P < 0.05$, Fig. 4*D*), suggesting that inputs at the edges of the FRA dominate the late portion of the response. In contrast, the onset and termination responses of cKO units were positively correlated (median: +0.05, signed rank $P < 0.05$, Fig. 4*D*), indicating that the same FRA regions tend to be active throughout the response. The correlations for the two groups are significantly different (medians: CT = −0.05, cKO = +0.05, rank sum $P < 0.01$, Fig. 4*D*). Therefore, cKO units do not appear to develop responses at the edge of the FRA over time as control units do. Combined with the decrease in response area and lack of long-latency responses, this result reinforces the idea that only central, TC-driven responses remain in the FRAs of cKO units.

Dlx1$^{-/f}$;I12b-Cre Cortical Responses Are Less Sparse. To explore changes in firing rate, we determined the response rate as a function of stimulus intensity for tones near CF (±0.2

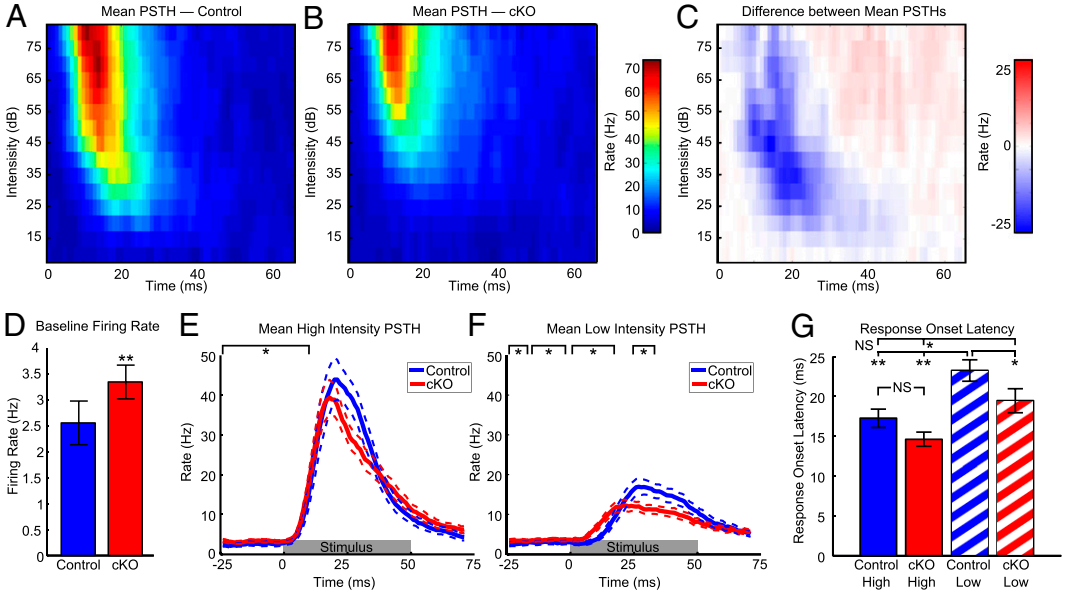

Fig. 3. Long latency responses are absent near threshold in cKO mice. (*A* and *B*) Population mean PSTH near CF at various intensities for auditory cortical units. (*C*) Difference, cKO − control. (*D*) Baseline firing rates (50 ms preceding the stimulus; medians: CT 1.11 and cKO 2.38, $P < 0.005$). (*E* and *F*) Population mean PSTH at high (60–80 dB) and low intensities (threshold ±10 dB) near CF (±0.2 octaves, dotted lines are ± SEM). Black brackets, area with five or more consecutive samples with rank sum $P < 0.05$. Gray bar, stimulus. (*G*) Onset latency per unit at high and low intensities (*$P < 0.05$, **$P < 0.01$, all Bonferonni corrected, $n = 54$ control and 58 cKO).

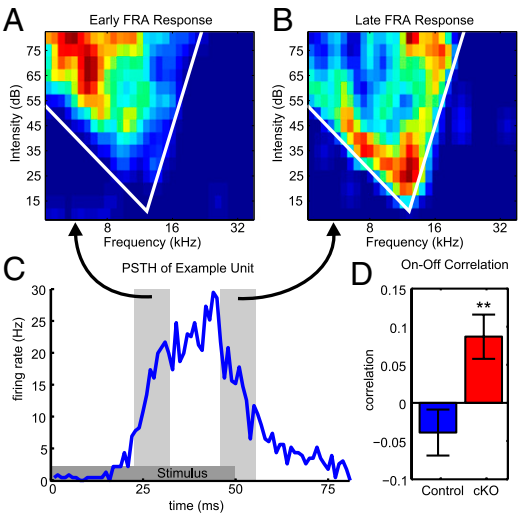

Fig. 4. Early and late responses are similar in cKO but not in control mice. (*A* and *B*) Onset FRA (*A*) and termination FRA (*B*) from a control unit (correlation = −0.37). White lines, size of the entire response FRA. (*C*) PSTH of the unit in *A* and *B*. Light gray bars, early and late response windows, respectively. Dark gray bar, stimulus. (*D*) Correlations of early and late responses (medians: CT = −0.05 and cKO = 0.05, $P < 0.005$, $n = 54$ and 58).

octaves) also known as the rate-level function (RLF, Fig. 5*A*). For individual units, the response magnitudes near CF were not significantly different between groups (at 80 dB: medians, CT =13 Hz and cKO = 15 Hz, $P = 0.40$, Fig. 5*B*, see *SI Results* for ANOVA). In contrast, the multiunit responses of cKO mice were 50% stronger (at 80 dB: medians, CT = 48 Hz and cKO = 73 Hz, $P < 0.001$, $n = 88$ and 96, Fig. 5*D*, see *SI Results* for ANOVA and thalamic data). Because the response rates of individual units were not different but more multiunit events were observed at each site, it is likely that the number of individual units simultaneously active in response to tones increased in cKO mice. Therefore, responses were less sparse following the loss of DTIs.

The decrease in sparseness, abnormal EEG activity, and increase in baseline firing rate are the only data in agreement with pharmacological blockades of inhibition (6–12). Previous studies

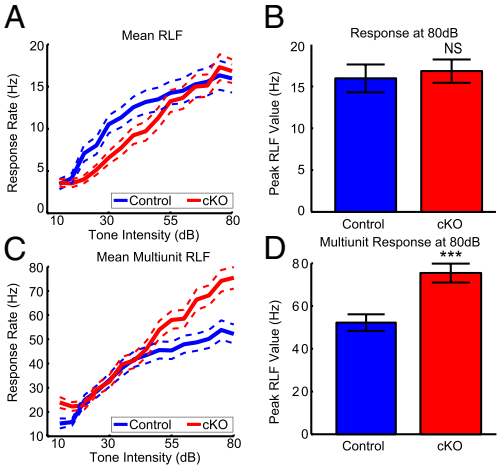

Fig. 5. Cortical responses of cKO mice are less sparse. (*A*) Mean RLFs for single cortical units (dotted lines, ±SEM). (*B*) Response magnitude of single units for 80-dB stimuli ($P = 0.37$, $n = 54$ control and 58 cKO). (*C*) Mean RLFs for cortical multiunits (dotted lines, ±SEM). (*D*) Response magnitude of multiunits for 80-dB stimuli ($P < 0.001$, $n = 88$ control and 96 cKO).

demonstrated that acute reductions of inhibition expand the breadth of receptive fields and lengthen cortical responses (6–12). We observed the opposite following the chronic decrease in inhibition and identified a selective decrease in responses at the edges of the receptive field. As overactivity is still present, it suggests that compensation occurs at the FRA edges to weaken and limit the spread of overactivity.

Discussion

We used *Dlx1*$^{-/f}$*;I12b-Cre* mutants (cKO) to study the effects of a partial loss of DTIs on auditory cortical processing. These animals have normal peripheral hearing but an ∼30% reduction in SOM$^+$, NPY$^+$, CR$^+$, and VIP$^+$ interneurons that develops after the end of the critical period in auditory cortex (Fig. 1). As SST and VIP are believed to be mutually exclusive interneuron markers in mouse cortex (1, 17) and derive from the medial and caudal ganglionic eminence progenitor populations, respectively (47–52), this demonstrates that interneurons from distinct progenitor pools are affected by the *Dlx1* mutation.

Loss of Functional Cortical–Cortical Connectivity in Dxl1$^{-/f}$;I12b-Cre Mice. After the loss of DTIs, we found that receptive field sizes were reduced in single units from core areas of auditory cortex in cKO mutants due to higher thresholds and narrower bandwidths (Fig. 2). We obtained evidence that this reduction does not occur in the thalamus and therefore emerges in cortex (Fig. S3). As descending cortical fibers can modulate subcortical function, it is possible that a more detailed investigation of subcortical activity may identify differences in Dlx1 mutants; however, the differences we observed in cortex do not appear to result directly from changes in thalamic processing. This cortical receptive field phenotype is in agreement with observations from the visual system of *Dlx1*$^{-/-}$ mice where the range of stimuli that drive responses is also reduced in most V1 cortical neurons and thalamic circuitry remains intact (36). This commonality suggests that the reduction in cortical receptive field size may be a general response to the loss of dendrite-targeting inhibition. In auditory cortex of cKO mice, the edges of the FRAs, which normally have long-latency responses, were absent (Figs. 2–4). Instead, the edges of cKO FRAs have response latencies comparable to short-latency, central responses of control units (Fig. 3). Furthermore, Control responses progress from the center to the edge in a patterned fashion; however, in cKO responses the central region is active at both the response onset and termination as if the longer-latency edge responses were absent (Fig. 4). The absent FRA edges are usually driven primarily by CC connectivity (42–44). Therefore, we propose that the decrease in receptive field size may be a change related to a decreased ability of CC connections to drive responses.

There are several possible mechanisms for this change, including decreased CC synaptic strength, different cell intrinsic properties of excitatory neurons, and compensatory changes in inhibitory circuitry. Weakened excitatory inputs have been observed in the hippocampus of *Dlx1*$^{-/-}$ mutants (33). The amplitude of inputs from excitatory neurons onto inhibitory interneurons decreases, but the rate of excitatory synaptic activity and intrinsic properties of the surviving interneurons were not affected by the loss of *Dlx1* (33). This result has two implications for the current work. First, the intrinsic electrical properties of the surviving interneuron populations appear to be unaffected by the loss of *Dlx1*. Second, *Dlx1* mutants compensate for the loss of inhibition by decreasing excitatory drive. If the amplitude of excitatory connections onto excitatory neurons in auditory cortex decreases in this manner, the expected outcome would be the reduction in CC-driven responses that we observed in cKO mutants. Another possibility is that the intrinsic properties of excitatory neurons could change to reduce the effectiveness of inputs, such as a decrease in the input resistance of dendrites. Alternatively, the remaining inhibitory

interneurons could increase the strength of their responses and overcompensate for the loss of DTIs, thereby suppressing normal CC activity. Computational modeling in V1 of *Dlx1* mice suggests this alternative (36). Regardless of the mechanism, the observed changes in cortical receptive fields will limit the complexity of network processing.

The reduction in edge responses may reflect compensation to reduce overactivity observed in cKO mice (Fig. 5 and Fig. S1). Whereas the number of single-unit spikes remained constant in auditory cortex in response to tones, the number of multiunit spikes increased by 50%, indicating that overactivity to normal stimuli develops following the loss of DTIs and responses become less sparse. Combined with the increase in baseline firing rates and seizure-like activity, these are the only results in agreement with acute, pharmacological disruptions of inhibition. Pharmacological blockades of inhibition have been shown to broaden spectral tuning, including lowering thresholds and revealing longer latency responses (6–12). However, the opposite results were observed in our study following the chronic disruption of dendrite-targeting inhibition and are likely to reflect compensation. Therefore, approaches that examine only the acute effects of reducing interneuron function are likely to be incomplete models of chronic human neurological conditions but remain valuable for determining the functional role of these circuit elements. If compensation in *Dlx1* mutants works to oppose acute changes, one could predict that acute inactivation of DTIs will selectively enhance the spectral edges of the receptive field driven by CC connections. The opposite, acute activation, would then be predicted to selectively suppress the spectral edges of the receptive field. Further studies are needed to test these hypotheses.

Role of Dendrite-Targeting Interneurons in Health and Disease. Reduction of inhibition is a component of many neurological conditions, including hearing loss, aging, TBI, and neuropsychiatric diseases (19–29). Following hearing loss, cortical response thresholds are higher at the affected frequencies and a subsequent loss of inhibition follows (25). This weakened inhibition has been linked with the perception of tinnitus (29). Tinnitus may develop as excitation and inhibition find a new balance following the reduction of inhibition. Dendrite-targeting interneurons are also lost selectively after TBI (24). Both TBI patients and *Dlx1* mutant mice display an increased susceptibility to seizures (24, 30). The cognitive symptoms in TBI patients may also be driven by the loss of DTIs. DTIs are also lost during aging, which may lead to progressive deficits in speech comprehension (19). Responsiveness to one component of speech, FM sweeps, relies on asymmetric CC connectivity and the response dynamics of both excitatory and inhibitory interneurons (14, 18, 53–55). The aging-induced loss of interneurons followed by a compensatory loss of excitatory CC inputs may contribute to deficits in speech comprehension. Compensatory mechanisms may account for many symptoms of complex neurological conditions.

The described long-term changes may reveal some of the normal function of DTIs. As DTIs are recruited by CC activity, they are well suited to mitigate overactivity (56). Also, DTIs target dendrites, where excitatory CC connections dominate (57–64) and respond to stimuli with similar timing as excitatory cortical neurons (65). Under healthy conditions, activity propagated by CC connectivity will elicit a sufficient inhibitory response to shape cortical responses and maintain a safe balance of excitation and inhibition. After the loss of DTIs, excitatory CC connections will be uninhibited but may subsequently weaken to normalize the overall level of excitation. This compensation would replicate a state of tonic DTI inhibition. Fitting with this hypothesis, responses normally driven by CC connections are lost in cKO mutants but signs of overactivity remain. When faced with overactivity, the nervous system may sacrifice connectivity and computational power for stability. Deficits in neurological conditions with reduced inhibition may reflect compensatory changes as well as the direct effects of interneuron losses. It is therefore necessary to study long-term compensatory mechanisms following the loss of specific interneuron populations to better understand human neurological conditions.

Methods

Experiments were performed on *Dlx1*$^{-/f}$;*I12b-Cre* and *Dlx*$^{+/f}$;*I12b-Cre* mice using procedures approved by the University of California San Francisco Institutional Animal Care and Use Committee and in accordance with National Institutes of Health guidelines. For details of the generation of these mice and histological verification see *SI Methods*.

Electrophysiology. EEG observations were made by using a time-locked video EEG monitoring system (Pinnacle Technology). For EEG recordings, mice were surgically implanted in the left and right frontal and parietal cortices with electrodes. Each mouse was anesthetized with isofluorane to an areflexive state. Head mounts were attached with conductive stainless steel screws to act as recording electrodes. Dental cement was used to secure the head mount, and animals were allowed to recover for 3–5 d before recording sessions were initiated. Differential EEGs were collected from 2-mo-old animals over 8-h recording sessions.

Auditory brainstem responses were assessed under ketamine and xylazine anesthesia. Silver wires were inserted through the skin on either side of the brainstem and the forehead. Event-related potential evoked by clicks at various intensities were recorded (TDT Sys3 with BioSigRP; Tucker Davis Technologies).

To collect extracellular recordings, male and female animals aged between p33 and p65 were anesthetized to areflexia with a mixture of ketamine and xylazine. A small craniotomy was then performed over auditory cortex. Primary auditory cortical areas were identified by a multiunit response latency of ∼10 ms (TDT Sys3 with Brainware; Tucker Davis Technologies). A frequency gradient reversal between A1 and AAF was not consistently observed in all control and mutant mice; therefore, a sampling was taken from midlow frequencies and short latency (<15 ms) areas. Auditory thalamus was identified as the auditory responsive region with latencies around 8 ms near the stereotactic coordinates 3.2 mm posterior, 1.9 mm lateral, and 3.0 mm ventral of Bregma. Extracellular recording traces were collected with 16-channel probes (NeuroNexus) on a 32-channel recording system (Neuralynx). Threshold crossings at 4 SD were collected as multiunit spikes and these were sorted offline using KlustaKwik (written by Ken Harris) followed by manual supervision to identify single-unit responses. Only single units and multiunit sites that contained more than 500 events and doubled their average firing rate in response to tones were analyzed.

Stimuli and Analysis. Tones spanning 4 octaves (4–32 kHz, 0.1 octave spacing) and 70 dB (10–80 dB, 5-dB spacing) lasting 50 ms were presented every 750 ms. In some experiments, tones were followed 70 ms later by a soft burst of white noise for purposes not discussed here. No significant differences in tone responses for the two conditions were observed and the data were pooled. However, we limited all analysis to action potentials that occurred less than 70 ms after tone onset. The FRA was determined as the areas above 1/4 peak response after subtracting the baseline. Threshold was determined as the lowest intensity bin in the FRA, and CF was the middle frequency bin at that intensity. Multiple intensity regions were selected over multiple spectral regions for the PSTH because the spectral edges of the tuning curve were sometimes at the edge of the frequency sampling space we tested and could not always be reconstructed with confidence. Response onset was estimated as the time to reach 1/2 of the peak response of the PSTH at that intensity. Response termination was the time point to fall to 1/2 of the peak value after the peak of the PTSH. When correlating the onset FRA and the termination FRA, 10-ms windows centered on both times were used and the original FRA was applied as a mask before the correlation was calculated.

Data analysis was performed in Matlab (MathWorks) using custom software. Unless otherwise noted, all statistical tests are nonparametric, Wilcoxon rank-sum tests. Therefore, data median data values are given in the text rather than means. However, for the purpose of display, the data are plotted as mean ± SEM. All units were used in each analysis (cKO: 58 cortical, 65 thalamic; CT: 54 cortical, 31 thalamic).

ACKNOWLEDGMENTS. B.A.S. and C.E.S. are supported by National Institutes of Health (NIH) Grants DC02260 and MH077970, the Coleman Memorial Fund, and Hearing Research, Inc.. B.A.S. is also supported by NIH Grant GM007449. A.S. is supported by NIH Grant MH089920. G.B.P. and J.L.R.R. are supported by Nina Ireland, Weston Havens Foundation, and NIH Grant MH049428. V.S.S and K.K.A.C. are supported by the Staglin Family, International Mental Health

Research Organization, NIH Grant MH085946, the Simons Foundation for Autism Research, a Steve and Connie Lieber/National Alliance for Research on Schizophrenia and Depression Young Investigator Award, and the Alfred P. Sloan Foundation. K.K.A.C. also supported by NIH Grant MH089920.

1. Markram H, et al. (2004) Interneurons of the neocortical inhibitory system. *Nat Rev Neurosci* 5:793–807.
2. Wu GK, Arbuckle R, Liu B-H, Tao HW, Zhang LI (2008) Lateral sharpening of cortical frequency tuning by approximately balanced inhibition. *Neuron* 58:132–143.
3. Wu GK, Li P, Tao HW, Zhang LI (2006) Nonmonotonic synaptic excitation and imbalanced inhibition underlying cortical intensity tuning. *Neuron* 52:705–715.
4. Tan AYY, Zhang LI, Merzenich MM, Schreiner CE (2004) Tone-evoked excitatory and inhibitory synaptic conductances of primary auditory cortex neurons. *J Neurophysiol* 92:630–643.
5. Wehr M, Zador AM (2003) Balanced inhibition underlies tuning and sharpens spike timing in auditory cortex. *Nature* 426:442–446.
6. Wang J, Caspary D, Salvi RJ (2000) GABA-A antagonist causes dramatic expansion of tuning in primary auditory cortex. *Neuroreport* 11:1137–1140.
7. Wang J, McFadden SL, Caspary D, Salvi R (2002) Gamma-aminobutyric acid circuits shape response properties of auditory cortex neurons. *Brain Res* 944:219–231.
8. Foeller E, Vater M, Kössl M (2001) Laminar analysis of inhibition in the gerbil primary auditory cortex. *J Assoc Res Otolaryngol* 2:279–296.
9. Chen QC, Jen PH (2000) Bicuculline application affects discharge patterns, rate-intensity functions, and frequency tuning characteristics of bat auditory cortical neurons. *Hear Res* 150:161–174.
10. Chang EF, Bao S, Imaizumi K, Schreiner CE, Merzenich MM (2005) Development of spectral and temporal response selectivity in the auditory cortex. *Proc Natl Acad Sci USA* 102:16460–16465.
11. Jen PH-S, Chen QC, Wu FJ (2002) Interaction between excitation and inhibition affects frequency tuning curve, response size and latency of neurons in the auditory cortex of the big brown bat, Eptesicus fuscus. *Hear Res* 174:281–289.
12. Müller CM, Scheich H (1988) Contribution of GABAergic inhibition to the response characteristics of auditory units in the avian forebrain. *J Neurophysiol* 59:1673–1689.
13. Froemke RC, Merzenich MM, Schreiner CE (2007) A synaptic memory trace for cortical receptive field plasticity. *Nature* 450:425–429.
14. Razak KA, Fuzessery ZM (2009) GABA shapes selectivity for the rate and direction of frequency-modulated sweeps in the auditory cortex. *J Neurophysiol* 102:1366–1378.
15. Kurt S, Crook JM, Ohl FW, Scheich H, Schulze H (2006) Differential effects of iontophoretic in vivo application of the GABA(A)-antagonists bicuculline and gabazine in sensory cortex. *Hear Res* 212:224–235.
16. Schulze H, Langner G (1999) Auditory cortical responses to amplitude modulations with spectra above frequency receptive fields: Evidence for wide spectral integration. *J Comp Physiol A Neuroethol Sens Neural Behav Physiol* 185:493–508.
17. Rudy B, Fishell G, Lee S, Hjerling-Leffler J (2011) Three groups of interneurons account for nearly 100% of neocortical GABAergic neurons. *Dev Neurobiol* 71:45–61.
18. Hughes LF, Turner JG, Parrish JL, Caspary DM (2010) Processing of broadband stimuli across A1 layers in young and aged rats. *Hear Res* 264:79–85.
19. Stanley EM, Fadel JR, Mott DD (2011) Interneuron loss reduces dendritic inhibition and GABA release in hippocampus of aged rats. *Neurobiology of Aging*. Available at http://www.ncbi.nlm.nih.gov/pubmed/21277654. Accessed November 27, 2011.
20. Gogolla N, et al. (2009) Common circuit defect of excitatory-inhibitory balance in mouse models of autism. *J Neurodev Disord* 1:172–181.
21. Fung SJ, et al. (2010) Expression of interneuron markers in the dorsolateral prefrontal cortex of the developing human and in schizophrenia. *Am J Psychiatry* 167: 1479–1488.
22. Hashimoto T, et al. (2008) Alterations in GABA-related transcriptome in the dorsolateral prefrontal cortex of subjects with schizophrenia. *Mol Psychiatry* 13:147–161.
23. Hashimoto T, et al. (2008) Conserved regional patterns of GABA-related transcript expression in the neocortex of subjects with schizophrenia. *Am J Psychiatry* 165: 479–489.
24. Lowenstein DH, Thomas MJ, Smith DH, McIntosh TK (1992) Selective vulnerability of dentate hilar neurons following traumatic brain injury: A potential mechanistic link between head trauma and disorders of the hippocampus. *J Neurosci* 12:4846–4853.
25. Kotak VC, et al. (2005) Hearing loss raises excitability in the auditory cortex. *J Neurosci* 25:3908–3918.
26. Sanes DH, Kotak VC (2011) Developmental plasticity of auditory cortical inhibitory synapses. *Hear Res* 279:140–148.
27. Sarro EC, Kotak VC, Sanes DH, Aoki C (2008) Hearing loss alters the subcellular distribution of presynaptic GAD and postsynaptic GABAA receptors in the auditory cortex. *Cereb Cortex* 18:2855–2867.
28. Takesian AE, Kotak VC, Sanes DH (2012) Age-dependent effect of hearing loss on cortical inhibitory synapse function. *J Neurophysiol* 107:937–947.
29. Yang S, Weiner BD, Zhang LS, Cho S-J, Bao S (2011) Homeostatic plasticity drives tinnitus perception in an animal model. *Proc Natl Acad Sci USA* 108:14974–14979.
30. Cobos I, et al. (2005) Mice lacking Dlx1 show subtype-specific loss of interneurons, reduced inhibition and epilepsy. *Nat Neurosci* 8:1059–1068.
31. Anderson SA, Eisenstat DD, Shi L, Rubenstein JL (1997) Interneuron migration from basal forebrain to neocortex: Dependence on Dlx genes. *Science* 278:474–476.
32. Panganiban G, Rubenstein JLR (2002) Developmental functions of the Distal-less/Dlx homeobox genes. *Development* 129:4371–4386.
33. Jones DL, Howard MA, Stanco A, Rubenstein JLR, Baraban SC (2011) Deletion of Dlx1 results in reduced glutamatergic input to hippocampal interneurons. *J Neurophysiol* 105:1984–1991.
34. Barkat TR, Polley DB, Hensch TK (2011) A critical period for auditory thalamocortical connectivity. *Nat Neurosci* 14:1189–1194.
35. Mao R, et al. (2009) Reduced conditioned fear response in mice that lack Dlx1 and show subtype-specific loss of interneurons. *J Neurodev Disord* 1:224–236.
36. Mao R, et al. (2012) Influence of a Subtype of Inhibitory Interneuron on Stimulus-Specific Responses in Visual Cortex. *Cerebral Cortex (New York, NY: 1991)* 22:493–508.
37. Cobos I, et al. (2005) Mice lacking Dlx1 show subtype-specific loss of interneurons, reduced inhibition and epilepsy. *Nat Neurosci* 8:1059–1068.
38. Polley DB, Cobos I, Merzenich MM, Rubenstein JLR (2006) Severe hearing loss in Dlxl mutant mice. *Hear Res* 214:84–88.
39. Qiu M, et al. (1997) Role of the Dlx homeobox genes in proximodistal patterning of the branchial arches: Mutations of Dlx-1, Dlx-2, and Dlx-1 and -2 alter morphogenesis of proximal skeletal and soft tissue structures derived from the first and second arches. *Dev Biol* 185:165–184.
40. Ghanem N, et al. (2007) Distinct cis-regulatory elements from the Dlx1/Dlx2 locus mark different progenitor cell populations in the ganglionic eminences and different subtypes of adult cortical interneurons. *J Neurosci* 27:5012–5022.
41. Potter GB, et al. (2009) Generation of Cre-transgenic mice using Dlx1/Dlx2 enhancers and their characterization in GABAergic interneurons. *Mol Cell Neurosci* 40:167–186.
42. Kaur S, Lazar R, Metherate R (2004) Intracortical pathways determine breadth of subthreshold frequency receptive fields in primary auditory cortex. *J Neurophysiol* 91: 2551–2567.
43. Kaur S, Rose HJ, Lazar R, Liang K, Metherate R (2005) Spectral integration in primary auditory cortex: Laminar processing of afferent input, in vivo and in vitro. *Neuroscience* 134:1033–1045.
44. Happel MFK, Jeschke M, Ohl FW (2010) Spectral integration in primary auditory cortex attributable to temporally precise convergence of thalamocortical and intracortical input. *J Neurosci* 30:11114–11127.
45. Schreiner C, Wong S, Dinse H (2006) in *Listening to Speech: an Auditory Perspective*, eds Greenberg S, Ainsworth W (Lawrence Erlbaum Associates, Mahwah, NJ), pp 129–141.
46. Moller AR (1975) Latency of unit responses in cochlear nucleus determined in two different ways. *J Neurophysiol* 38:812–821.
47. Butt SJB, et al. (2005) The temporal and spatial origins of cortical interneurons predict their physiological subtype. *Neuron* 48:591–604.
48. De Marco García NV, Karayannis T, Fishell G (2011) Neuronal activity is required for the development of specific cortical interneuron subtypes. *Nature* 472:351–355.
49. Lee S, Hjerling-Leffler J, Zagha E, Fishell G, Rudy B (2010) The largest group of superficial neocortical GABAergic interneurons expresses ionotropic serotonin receptors. *J Neurosci* 30:16796–16808.
50. Miyoshi G, Butt SJB, Takebayashi H, Fishell G (2007) Physiologically distinct temporal cohorts of cortical interneurons arise from telencephalic Olig2-expressing precursors. *J Neurosci* 27:7786–7798.
51. Miyoshi G, et al. (2010) Genetic fate mapping reveals that the caudal ganglionic eminence produces a large and diverse population of superficial cortical interneurons. *J Neurosci* 30:1582–1594.
52. Fogarty M, et al. (2007) Spatial genetic patterning of the embryonic neuroepithelium generates GABAergic interneuron diversity in the adult cortex. *J Neurosci* 27: 10935–10946.
53. Mendelson JR, Ricketts C (2001) Age-related temporal processing speed deterioration in auditory cortex. *Hear Res* 158:84–94.
54. Mendelson JR, Lui B (2004) The effects of aging in the medial geniculate nucleus: A comparison with the inferior colliculus and auditory cortex. *Hear Res* 191:21–33.
55. Zhang LI, Tan AYY, Schreiner CE, Merzenich MM (2003) Topography and synaptic shaping of direction selectivity in primary auditory cortex. *Nature* 424:201–205.
56. Silberberg G, Markram H (2007) Disynaptic inhibition between neocortical pyramidal cells mediated by Martinotti cells. *Neuron* 53:735–746.
57. Wang Y, et al. (2004) Anatomical, physiological and molecular properties of Martinotti cells in the somatosensory cortex of the juvenile rat. *J Physiol* 561:65–90.
58. Bayraktar T, Welker E, Freund TF, Zilles K, Staiger JF (2000) Neurons immunoreactive for vasoactive intestinal polypeptide in the rat primary somatosensory cortex: Morphology and spatial relationship to barrel-related columns. *J Comp Neurol* 420: 291–304.
59. Peters A, Meinecke DL, Karamanlidis AN (1987) Vasoactive intestinal polypeptide immunoreactive neurons in the primary visual cortex of the cat. *J Neurocytol* 16: 23–38.
60. Peters A, Kimerer LM (1981) Bipolar neurons in rat visual cortex: A combined Golgi-electron microscope study. *J Neurocytol* 10:921–946.
61. Kawaguchi Y, Kubota Y (1996) Physiological and morphological identification of somatostatin- or vasoactive intestinal polypeptide-containing cells among GABAergic cell subtypes in rat frontal cortex. *J Neurosci* 16:2701–2715.
62. Kawaguchi Y, Kubota Y (1997) GABAergic cell subtypes and their synaptic connections in rat frontal cortex. *Cereb Cortex* 7:476–486.
63. Melchitzky DS, Lewis DA (2008) Dendritic-targeting GABA neurons in monkey prefrontal cortex: Comparison of somatostatin- and calretinin-immunoreactive axon terminals. *Synapse* 62:456–465.
64. Peters A (1990) The axon terminals of vasoactive intestinal polypeptide (VIP)-containing bipolar cells in rat visual cortex. *J Neurocytol* 19:672–685.
65. Ma WP, et al. (2010) Visual representations by cortical somatostatin inhibitory neurons—selective but with weak and delayed responses. *J Neurosci* 30:14371–14379.

Supporting Information

Seybold et al. 10.1073/pnas.1205909109

SI Results

Abnormal EEG Activity in Conditional Knockout (cKO) Mutants. cKO mutants displayed abnormal EEG activity similar to *Dlx1*$^{-/-}$ mice. *Dlx1*$^{-/-}$ mice develop epilepsy after p30 (1); however, partial hearing loss can increase susceptibility to audiogenic seizures (2–4). EEG recordings showed that cKO mutants displayed abnormal, seizure-like EEG activity even though their peripheral hearing is normal. The events we observed were recorded in 8-h sessions in three 2-mo-old animals, an age when seizures are only starting to develop in *Dlx1*$^{-/-}$ mice. The events we observed were of short duration (~4 s, Fig. S1*C*), but longer than interictal spikes, which were also observed. These events were isolated to single channels and therefore not artifacts due to movement.

1. Cobos I, et al. (2005) Mice lacking Dlx1 show subtype-specific loss of interneurons, reduced inhibition and epilepsy. *Nat Neurosci* 8:1059–1068.
2. Van Middlesworth L, Norris CH (1980) Audiogenic seizures and cochlear damage in rats after perinatal antithyroid treatment. *Endocrinology* 106:1686–1690.
3. Kwon J, Pierson M (1997) Fos-immunoreactive responses in inferior colliculi of rats with experimental audiogenic seizure susceptibility. *Epilepsy Res* 27:89–99.
4. Pierson MG, Swann J (1991) Ontogenetic features of audiogenic seizure susceptibility induced in immature rats by noise. *Epilepsia* 32:1–9.

Detail of ANOVA for Testing Bandwidth. Bandwidths were tested in 5-dB steps up to 30 dB above threshold in cortex. Bandwidths were narrower over the range tested (two-way ANOVA, probability of a null main effect of the knockout, $P < 0.001$; probability for null interaction with stimulus intensity above threshold, 0.99).

Details of ANOVA for Rate Level Functions (RLFs). To complement the comparison of responses at a single, high intensity, we also compared responses at intensities relative to threshold for each unit. As predicted by the increased threshold in cKO units, control and cKO RLFs are significantly different (two-way ANOVA, probability of null main effect of the knockout, $P < 0.001$; probability for null interaction with stimulus intensity above threshold, $P = 0.41$). There are no significantly different intensity levels with Tukey–Kramer corrected t tests. Because thresholds vary from unit to unit, it is only meaningful to compare the entire RLF directly by aligning the RLFs at the threshold for each unit. In agreement with the effect observed at 80 dB, there is no difference between control and cKO single-unit responses at any intensity once aligned by threshold (two-way ANOVA, probability of null main effect of the knockout, $P = 0.30$; probability for null interaction with stimulus intensity above threshold, $P = 0.99$, Fig. S4*A*). In contrast, cKO multiunit responses are still different from control responses after aligning by threshold (two-way ANOVA, probability of null main effect of knockout, $P < 0.001$; probability of an interaction with stimulus intensity above threshold, $P = 0.15$, Fig. S4*B*).

We also examined RLFs from thalamic units. As predicted by the small decrease in threshold of cKO thalamic units, control and cKO RLFs are different (two-way ANOVA, probability of null main effect of the knockout, $P < 0.01$; probability for null interaction with stimulus intensity above threshold, $P = 0.98$, Fig. S4*C*). The main effect of the knockout is not changed by removing the characteristic frequency (CF) = 21 kHz outlier as in Fig. S3 ($P < 0.01$). This could result from a lack of descending cortical input via the nucleus of the reticular thalamus. However, this again appears to be merely a change in threshold. Neither control nor cKO thalamic single units were different once aligned by threshold (two-way ANOVA, probability of null main effect of the knockout, $P = 0.28$; probability for null interaction with stimulus intensity above threshold, $P = 0.90$, Fig. S4*D*).

SI Methods

Generation of Mice. The generation and characterization of *I12b-Cre* transgenic mice and *Dlx1* constituent mutant alleles was described previously (1, 2). To generate the conditional (floxed) allele of *Dlx1* (*Dlx1*^{f}), A targeting vector was generated that inserted a loxP sequence and Flippase Recognition Target (FRT)-flanked neomycin resistance gene cassette into the BamHI site in the first intron of *Dlx1* and a loxP sequence into the first XhoI site in the 3′ untranslated region. A TK cassette outside of the homologous arms was used for negative selection. The targeting vector was linearized with PvuI and transfected into JM1 ES cells. Clones were selected with G418 and ganciclovir. Clones were screened for homologous recombination by Southern blot and PCR. Two clones were identified with correct recombination events and expanded for blastocyst injection (~1% recombination efficiency). Chimeric mice were crossed with C57BL/6 wild-type mice, and germline transmission of the floxed Dlx1 allele was confirmed by PCR on genomic DNA extracted from mouse tails. Floxed Dlx1 mice were bred with flippase recombinase (FLP)-deleter mice purchased from Jackson Labs to remove the neomycin cassette, and removal of the neomycin gene was confirmed by PCR. The floxed Dlx1 allele (*Dlx1*^{f}) without the neomycin cassette was used for subsequent experiments. Floxed Dlx1 mice are genotyped by PCR: Dlx1_loxP_forward, CTC TCT TCT GGT GCC CTG TCA TTT CT; Dlx1_loxP_reverse, TCA CCG AAT CTC CCT GTG CTT TGA. The wild-type allele is ~338 bp and floxed allele is ~400 bp. *Dlx1*$^{f/-}$; *I12b-Cre* mutant and *Dlx1*$^{f/+}$;I12b-Cre controls were generated by crossing mice with floxed *Dlx1* alleles to mice carrying the *I12b-Cre* transgene in a *Dlx1* heterozygous background. Mouse colonies were maintained at the University of California, San Francisco (UCSF), in accordance with National Institutes of Health and UCSF guidelines.

1. Cobos I, et al. (2005) Mice lacking Dlx1 show subtype-specific loss of interneurons, reduced inhibition and epilepsy. *Nat Neurosci* 8:1059–1068.
2. Potter GB, et al. (2009) Generation of Cre-transgenic mice using Dlx1/Dlx2 enhancers and their characterization in GABAergic interneurons. *Mol Cell Neurosci* 40:167–186.

Histology. Adult *Dlx1*$^{f/-}$;*I12b-Cre* and *Dlx1*$^{f/+}$;*I12b-Cre* littermate mice were deeply anesthetized with avertin (Sigma; 0.2 mL/10 g body weight) and perfused intracardially with 4% (wt/vol) paraformaldehyde (PFA) in PBS solution (PBS 0.1 M, pH 7.4). The brains were removed and postfixed overnight in the same fixative, except brains prepared for vasoactive intestinal peptide (VIP) immunohistochemistry that where fixed for 30 min. Brain sections were prepared at a thickness of 50 μm on a vibratome and used for free-floating immunohistochemistry. The slices were washed in PBS solution, incubated in blocking solution [0.5% (vol/vol) Triton X-100, 10% (vol/vol) normal goat serum, 2% (vol/vol) nonfat milk, 0.2% gelatin in PBS] for 1 h, and incubated overnight at 4 °C in the primary antibody diluted in 0.5% Triton X-100, 3% normal goat serum, 0.2% gelatin in PBS. The antibodies used were as follows: calretinin polyclonal antibodies (1:500; Millipore), neuropeptide Y (NPY) polyclonal antibodies (1:250; ImmunoStar), parvalbumin monoclonal antibodies (1:500; Millipore), somatostatin monoclonal antibodies (1:250; Millipore), and VIP polyclonal antibodies (1:200; ImmunoStar). Immunoreactivity was detected with appropriate Alexa-488 or Alexa-594 (1:300; Molecular Probes) conjugated secondary antibodies. Quantifica-

tion of calretinin$^+$, NPY$^+$, parvalbumin$^+$, somatostatin$^+$, and VIP$^+$ cells in the primary auditory cortex was determined in coronal sections from three mice of each genotype. Cell counts were performed on digitized images obtained with a CoolSNAP EZ Turbo 1394 digital camera (Photometric) on a Nikon ECLIPSE 80i microscope (Nikon Instruments) using a 4× objective. The numbers of positive cells were assessed in a 1 mm^2 area of primary auditory cortex.

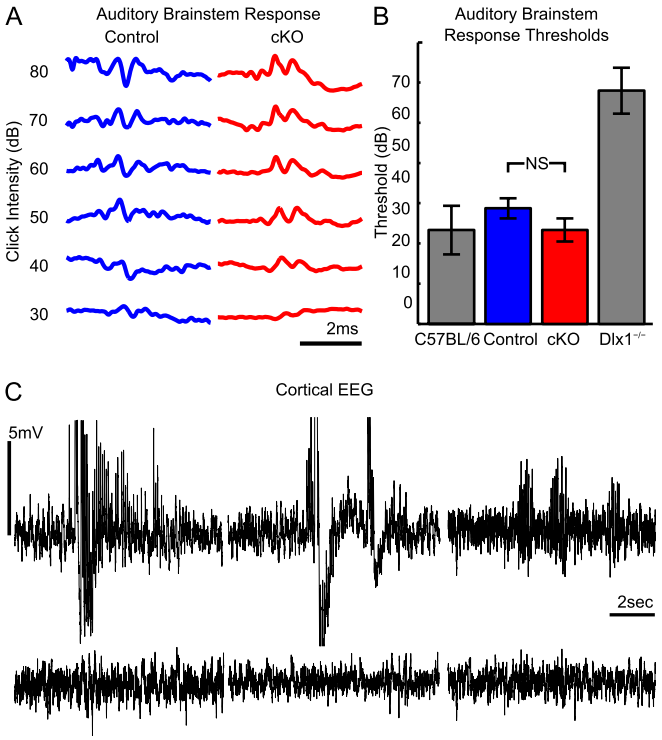

Fig. S1. Auditory brainstem responses are normal and seizure-like activity is observed by EEG in cKO mice. (*A*) Auditory brainstem responses (ABRs) from control and cKO mice. (*B*) ABR thresholds from control and cKO mice ($P > 0.05$, $n = 4$ and 3). For comparison purposes, data from C57BL/6 mice and previously reported values from a constitutive *Dlx1*$^{-/-}$ mutant are shown (1). (*C*) Abnormal EEG activity observed in cKO mice. *Upper*, three different episodes from two animals. *Lower*, simultaneous signals on other channels.

1. Polley DB, Cobos I, Merzenich MM, Rubenstein JLR (2006) Severe hearing loss in Dlxl mutant mice. *Hear Res* 214:84–88.

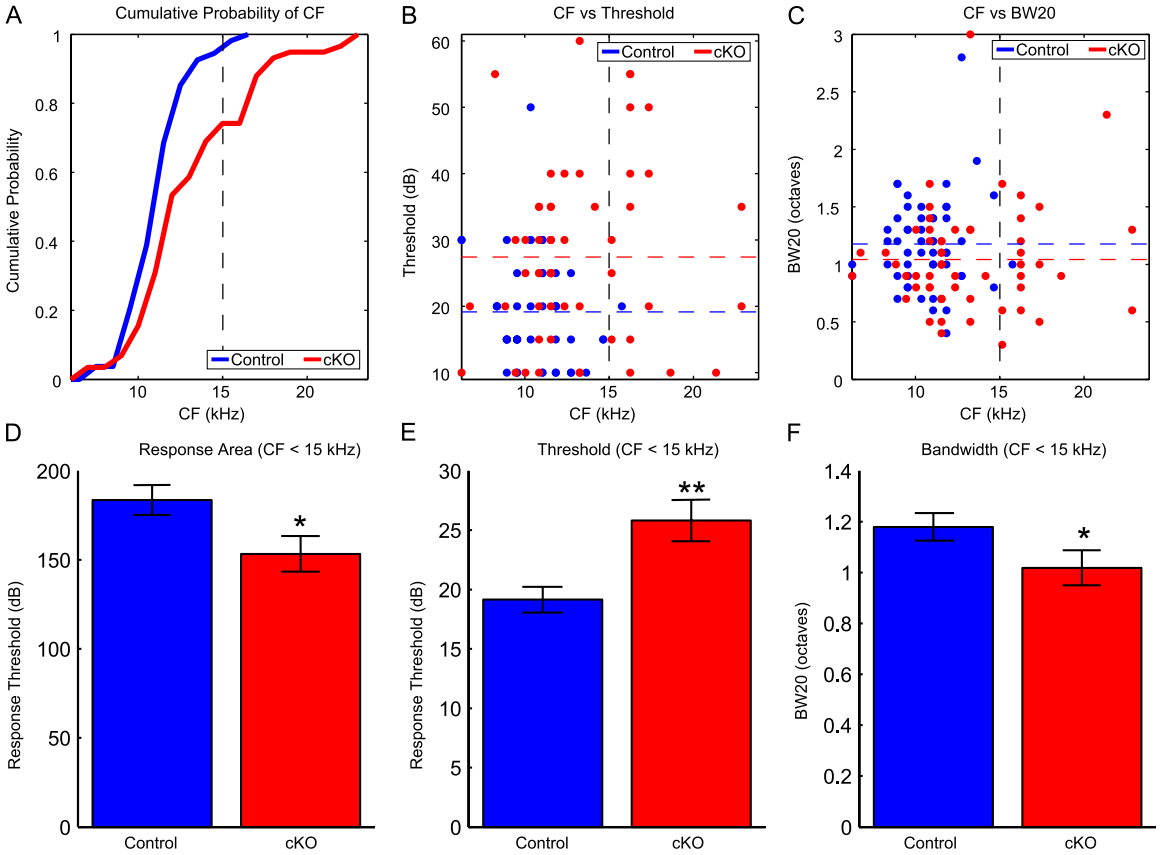

Fig. S2. Cortical responses are significantly different across similar frequencies. (*A*) Distribution of CFs recorded in control and cKO mutant mice. Vertical dashed line at 15 kHz used as the cutoff for similar frequency distributions. (*B*) Threshold as a function of CF. Horizontal dashed lines indicate population means. Vertical dashed line as in *A*. (*C*) Bandwidth at 20 dB above threshold as a function of CF. Dashed lines as in *B*. (*D*) Response areas from units with CFs less than 15 kHz are significantly smaller in cKO units (medians: control (CT), 179 dB*octaves and cKO, 169 dB*octaves; $P < 0.05$, $n = 53$ and 43). (*E*) Thresholds from units with CFs less than 15 kHz are significantly higher in cKO mutants (medians: CT, 20 dB and cKO, 25 dB; $P < 0.01$, $n = 53$ and 43). (*F*) Bandwidths 20 dB above threshold from units with CFs less than 15 kHz are significantly narrower in cKO units (medians: CT, 1.1 octaves and cKO, 1.0 octaves; $P < 0.05$, $n = 53$ and 43).

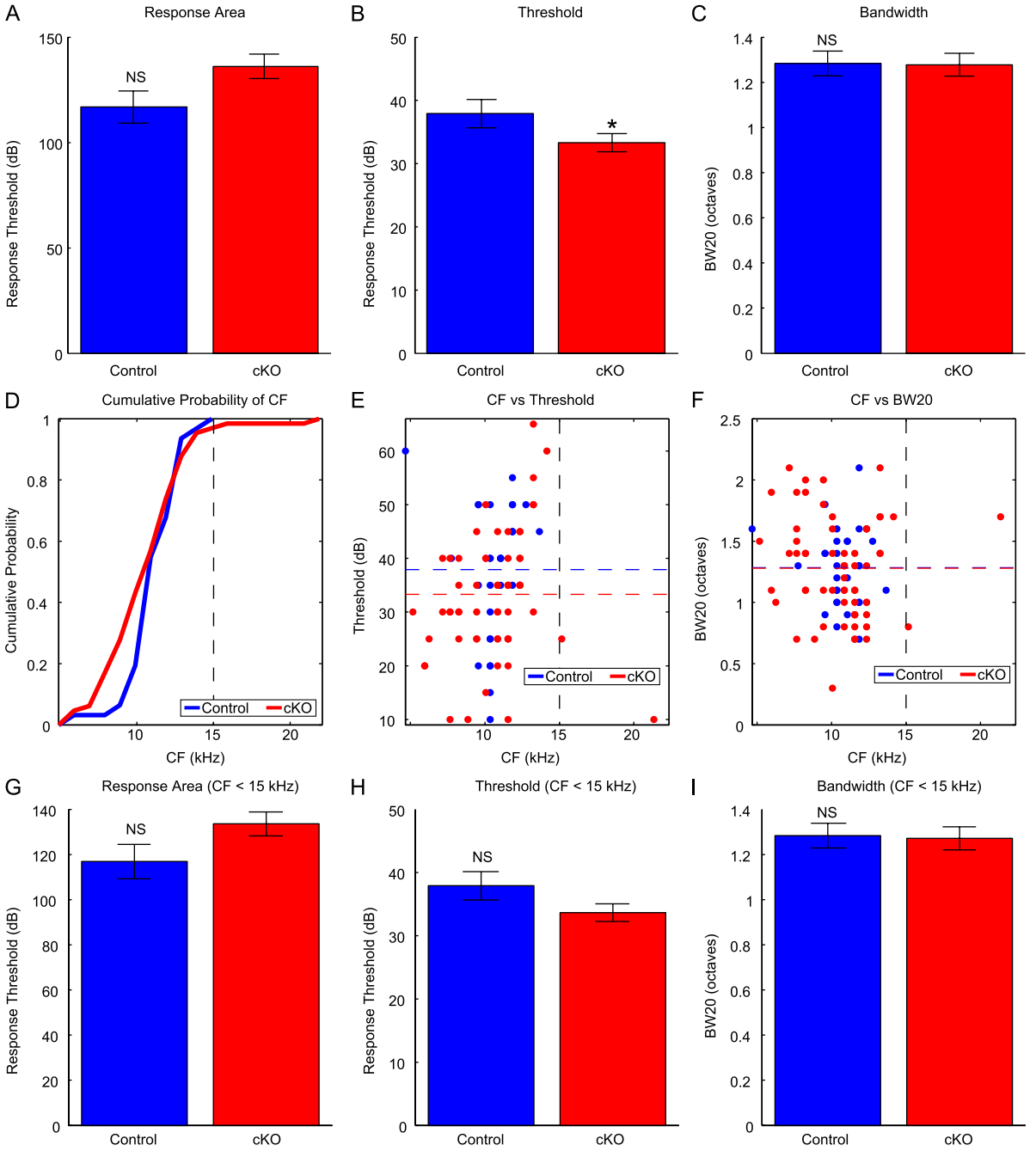

Fig. S3. Thalamic responses show little difference due to the loss of cortical interneurons. (*A*) Response areas are not significantly different in thalamus (medians: CT, 109 dB*octaves and cKO, 142 dB*octaves; $P = 0.06$, $n = 31$ and 65). Plot is identical to Fig. 2*H*. (*B*) Response thresholds are lower in cKO thalamus (medians: CT, 40 dB and cKO, 35 dB; $P = 0.049$, $n = 31$ and 65). Note: this is the opposite of the change observed in cortex and therefore cannot directly give rise to the results observed in cortex. Furthermore, this result is dependent on an outlier of the CF distribution (see *E* and *H*). If true, one possible explanation for lower thalamic thresholds is that inhibitory feedback from the nucleus of the reticular thalamus will decrease due to a decrease in low-threshold, excitatory, cortical inputs to that nucleus (1). (*C*) Bandwidths 20 dB above threshold are not significantly different in thalamus (medians: CT, 1.3 octaves and cKO, 1.3 octaves; $P = 0.91$, $n = 31$ and 65). (*D*) Distribution of CFs recorded in the thalamus of control and cKO mutant mice. Vertical dashed line at 15 kHz used as a cutoff for similar frequency distributions. Only one cKO unit (at 21 kHz) is beyond this cutoff. (*E*) Threshold as a function of CF. Dashed lines as in Fig. S2. (*F*) Bandwidth at 20 dB above threshold as a function of CF. Dashed lines as in *E*. (*G*) Response areas from thalamic units with CFs less than 15 kHz are not significantly different (medians: CT, 109 dB*octaves and cKO, 142 dB*octaves; $P = 0.07$, $n = 31$ and 64). (*H*) Thresholds from units with CFs less than 15 kHz are not significantly different (medians: CT, 40 dB and cKO, 35 dB; $P = 0.051$, $n = 31$ and 64). (*I*) Bandwidths 20 dB above threshold are not different (medians: CT, 1.3 octaves and cKO, 1.3 octaves; $P = 0.83$, $n = 31$ and 64).

1. Yu X-J, Meng X-K, Xu X-X, He J (2011) Individual auditory thalamic reticular neurons have large and cross-modal sources of cortical and thalamic inputs. *Neuroscience* 193:122–131.

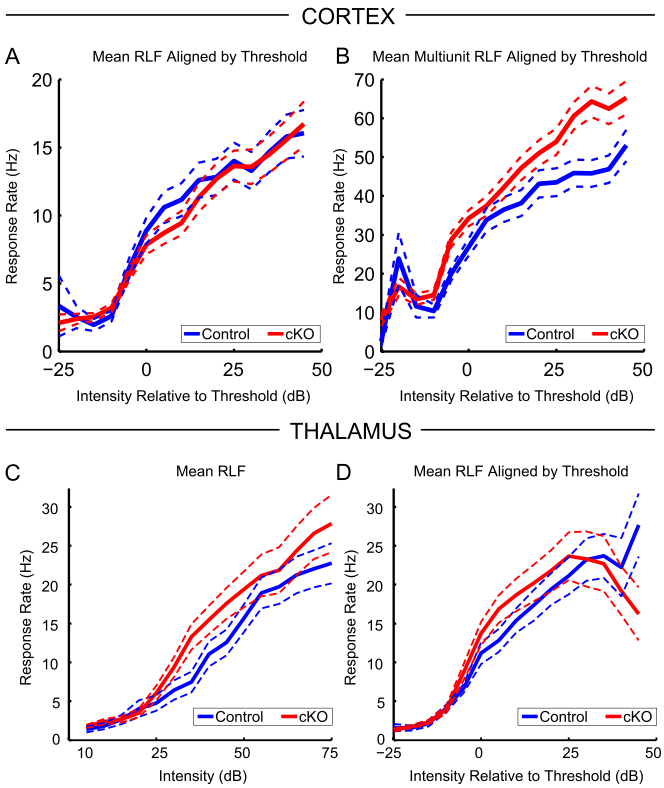

Fig. S4. Cortical responses of cKO mice are less sparse even when aligned by threshold. (*A*) Mean RLFs for single cortical units aligned by threshold for each unit (dotted lines ± SEM). (*B*) Mean RLFs for cortical multiunits aligned by threshold for each unit (dotted lines: ± SEM). (*C*) Mean RLFs for single thalamic units (dotted lines ± SEM). (*D*) Mean RLFs for single thalamic units aligned by threshold for each unit (dotted lines ± SEM).

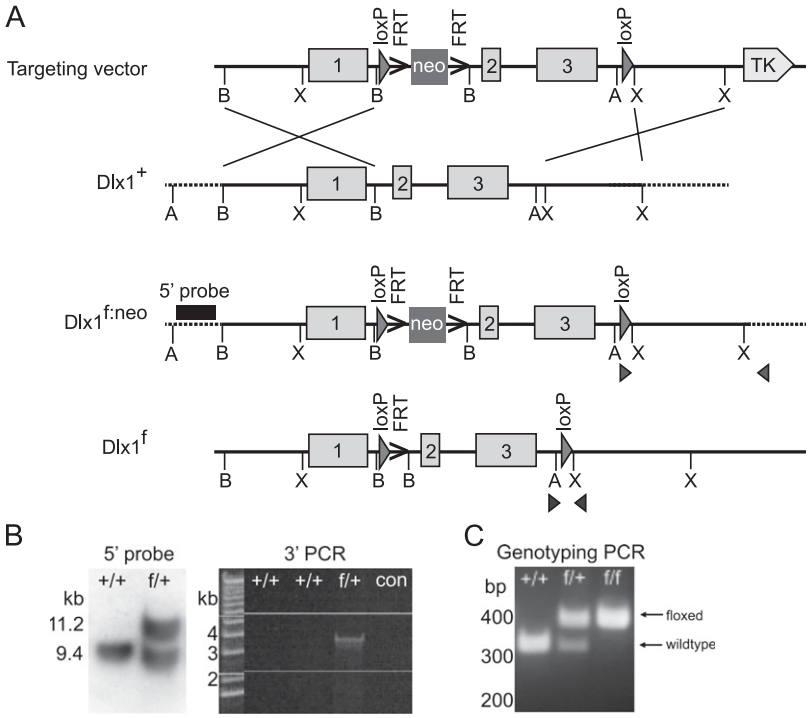

Fig. S5. Gene targeting to generate floxed *Dlx1*. (*A*) Schematic representation, from top to bottom, of the targeting vector, the wild-type Dlx1 allele (*Dlx1*$^{+}$), the conditional *Dlx1* allele before (*Dlx1*$^{f:neo}$), and after (*Dlx1*^{f}) removal of the neoselection cassette by Flp recombinase. A, AseI; B, BamHI; X, XhoI; Neo, neomycin resistance cassette; TK, herpes simplex virus thymidine kinase gene. Black triangle, loxP site; open arrowhead, FRT site. *Dlx1* exons (1–3) are shown as boxes. Small arrowheads represent PCR primers. The loxP sites were placed to flank exons 2 and 3, which together encode for the homeobox domain. (*B*, *Left*) Southern blot of genomic DNA extracted from transfected ES cells, digested with AseI, and visualized with the 5′ probe depicted in *A*. (*Right*) Long-range PCR of the 3′ arms between the loxP site in *Dlx1* to outside the targeting vector. +/+, wild-type DNA; f/+, recombinant clone; con, negative control. (*C*) PCR of tail genomic DNA for the 3′ loxP site shows wild-type, heterozygous, and homozygous floxed *Dlx1* mice.